Inorganic Chemistry

Article

pubs.acs.org/IC

Synthesis of PbS/PbI_2 Nanocomposites in Mixed Solvent and Their Composition-Dependent Electrogenerated Chemiluminescence Performance

Suli Liu, Long Zhang, Yanrong Li, Min Han, Zhihui Dai,* and Jianchun Bao*

Jiangsu Key Laboratory of Biofunctional Materials, School of Chemistry and Materials Science, Nanjing Normal University, Nanjing 210023, P. R. China

Supporting Information

ABSTRACT: PbS/PbI_2 nanocomposites were prepared by choosing $K[PbI_3]$ as both a lead salt and an iodide precursor and acetone/water as a reaction medium. It was found that the amount of the PbI_2 component could be controlled, to some extent, by varying the amount of water used. Further, this simple bicomponent precursor-based synthetic route can be extended to prepare other lead-containing nanocomposites such as Pb_3O_4/PbI_2 and $PbSe/PbI_2$. Because of the heavy-atom effect, PbS/PbI_2 nanocomposites exhibited good and composition-dependent electrogenerated chemiluminescence (ECL) performance, demonstrating their potential in the development of novel ECL sensors for analytical and clinical applications. These interesting findings would encourage us to gain deep insight on these phenomena, which could lead to the further development of these new inorganic materials and their applications.

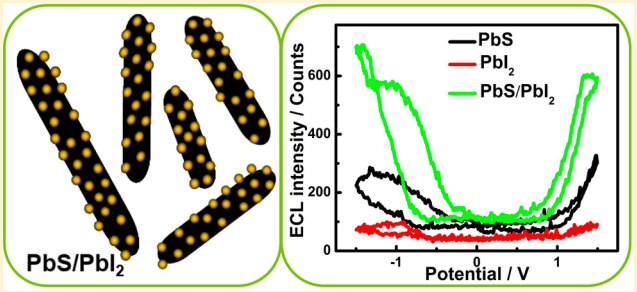

1. INTRODUCTION

Over the past decade, semiconductor nanocrystals have been extensively investigated because of their novel properties and potential uses in microelectronics, optoelectronics, light-to-energy conversion, photocatalysis, chemical sensing, and biological fluorescence labeling.[1−3] Control of the nanocrystal size and shape is required to tune their optical and electrical properties through changes in the band gap and/or carrier mobility.[4,5] The combination of several nanomaterials to form a semiconductor alloy/composite system represents another interesting approach to the creation of functional nanostructures with enhanced tunability of their structures and properties.[6−8] These hybrid nanocomposites inherit some of the properties of their components and often provide new and enhanced magnetic,[9] electrical,[10] optical,[11] and catalytic properties[12,13] through synergistic effects between components. For example, TiO_2−PbS heterojunctions absorb visible light well and exhibit good electron-transfer properties.[14] Modification of the surfaces of ZnO nanostructures with CdS enhances their ultraviolet photoconductivity[15] and results in a composite material with high, stable photocatalytic activity for splitting water into hydrogen.[16] Recent developments in materials chemistry have allowed many multicomponent semiconductor-based nanostructures to be prepared through different methods, such as heteroepitaxial hot injection,[17,18] two-stage cation exchange,[19,20] and seed-growth.[21,22] Despite these successes, exploiting simple synthetic strategies for the fabrication of new nanocomposites remains a challenging task.

Lead sulfide (PbS) has attracted considerable attention as an optoelectronic functional material with a near-infrared (NIR) band gap of 0.37 eV. Lead iodide (PbI_2) is an intrinsic wide-band-gap (>2 eV) semiconductor with applications in room temperature photocells, X-ray imaging, and γ-ray detectors.[23] The NIR-emitting carrier multiplication (transient absorption spectroscopy) of PbS quantum dots[24] and the UV−vis absorption and Raman spectra of PbI_2 nanoparticles[25−27] have been studied extensively. Although many PbS-based composites have been reported, to date, the study of PbS/PbI_2 nanocomposites, in which the S atom is replaced with the heavy I atom, has not yet been reported. The introduction of a heavy atom might have unexpected property and application. In this work, a facile bicomponent precursor-based route to PbS/PbI_2 nanocomposites is reported. We combined the use of $K[PbI_3]$ as a lead salt and an iodide precursor and acetone/water as a reaction medium for the fabrication of PbS/PbI_2 nanocomposites. It was found that the amount of the PbI_2 component could be controlled, to some extent, by varying the amount of water used. The PbS/PbI_2 nanocomposites exhibited excellent and composition-dependent electrogenerated chemiluminescence (ECL) performance, demonstrating their potential in the development of novel ECL sensors for analytical and clinical applications. Further, this simple synthetic method is extendable to prepare other lead-containing nanocomposites and is of great importance for the design and fabrication of advanced functional materials.

Received: May 17, 2014
Published: August 1, 2014

   dx.doi.org/10.1021/ic501128n | Inorg. Chem. 2014, 53, 8548−8554

2. EXPERIMENTAL SECTION

2.1. Synthesis. In a typical synthesis, a solution of tartaric acid was prepared by dissolving 0.024 g (0.1 mmol) of tartaric acid in 8 mL of acetone. Next, 0.2 g (0.3 mmol) of $K[PbI_3]\cdot 2H_2O$ was dissolved in the acetone solution under stirring at a bath temperature of 45 °C to form a light-yellow solution. Subsequently, 3 mL of 0.05 M thioacetamide (TAA) and 1 mL of 0.625 M NaOH aqueous solution were slowly added to the $K[PbI_3]$ solution under stirring. After these additions were complete, the color of the solution gradually turned from light yellow to gray and finally to black. The reactor was kept in a bath at 45 °C for 30 min and then naturally cooled to room temperature. The product was separated via centrifugation and washed with deionized water and ethanol three times. Finally, the product was dried under vacuum and used for further characterization, analysis, and property measurements. The volume ratio of acetone to water under typical conditions was 2:1. The recipes for changing the volume ratio of acetone-to-water to 5:1 and 1:1 are listed in Table S1 in the Supporting Information (SI).

For the synthesis of $PbSe/PbI_2$ nanocomposites, the recipe was similar to that of PbS/PbI_2 except that TAA was replaced with selenourea. For the synthesis of Pb_3O_4/PbI_2 nanocomposites, the recipe was similar to that of PbS/PbI_2 except that 3 mL of 0.05 M TAA and 1 mL of 0.625 M NaOH were replaced with $NH_3\cdot H_2O$ and the bath temperature of 45 °C was changed to 60 °C.

A total of 30 mg of the PbS/PbI_2 nanocomposites was dispersed in 10 mL of water to obtain a suspension of 3 mg mL^{-1} PbS/PbI_2 nanocomposites. The obtained suspension of 100 μL was then mixed with 5 μL of 3% Nafion to produce a PbS/PbI_2 nanocomposite colloid that was used for the following work.

2.2. Characterization. The X-ray diffraction (XRD) patterns were recorded using a powdered sample on a D/max 2500 VL/PC diffractometer (Japan) equipped with graphite-monochromatised Cu Kα radiation (λ = 1.54060 Å) at 2θ ranging from 10° to 90°. The corresponding working voltage and current were 40 kV and 100 mA, respectively. The X-ray energy-dispersive spectrometry (EDS) spectra were collected on a JSM-5610LV-Vantage-type energy spectrometer. The X-ray photoelectron spectroscopy (XPS) data were acquired on a scanning X-ray microprobe (PHI 5000 Verasa, Ulacphi, Inc.) using Al Kα radiation. The binding energies (BEs) of Pb 4f, S 2p, and I 3d were calibrated using the C 1s peak (BE = 284.6 eV) as a standard. Transmission electron microscopy (TEM) images were collected on a JEM-200CX instrument (Japan) using an accelerating voltage of 200 kV. High-resolution transmission electron microscopy (HRTEM) images were obtained at an accelerating voltage of 200 kV on a JEOL-2100F electron microscope equipped with EDS detectors for elemental mapping analyses. UV−vis measurements were made on a Varian Cary 5000 spectrophotometer at room temperature. The fluorescence spectra were measured on a PerkinElmer LS-50B spectrofluorimeter. The fluorescence lifetimes were determined by time-resolved intensity decay from the time-correlated single-photon-counting (TCSPC) method using a FM-4P-TCSPC instrument (Horiba Jobin Yvon FLUORCUBE). The excitation of the sample at 290 nm was achieved using a nanosecond diode laser as the light source. A total of 2 μL of a PbS/PbI_2 nanocomposite colloid solution was dropped on the pretreated glassy carbon electrode (GCE) surface and allowed to dry under ambient conditions for 3 h to produce a modified electrode. The ECL measurements were conducted using homemade ECL instrumentation containing a three-electrode system, i.e., modified GCEs as the working electrodes, a platinum counter electrode, and an Ag/AgCl reference electrode. ECL was measured by an ECL detection system (MPI-A, Remex Electronic Instrument High-Tech, Xi'an, China). The voltage of the photomultiplier tube was set at 800 V during detection.

3. RESULTS AND DISCUSSION

Figure 1 shows the XRD pattern of the sample prepared under the typical reaction conditions. The diffraction peaks at 2θ = 30.0, 43.0, 51.0, 62.5, 69.0, 71.1, and 78.9° can be indexed as cubic structure PbS (200), (220), (311), (400), (331), (420), and (422) faces (JCPDS 05-0592). The sharpness of the peaks indicates that the product is highly crystalline. Notably, a peak at 2θ = 34.2° is observed, which can be identified as hexagonal PbI_2 (JCPDS 07-0235). Additionally, some diffraction peaks, such as those at 2θ = 25.9, 53.3, and 84.6°, are attributed to either cubic PbS or hexagonal PbI_2 because of their identical characteristics. These XRD results indicate that the sample is composed of both PbS and PbI_2.

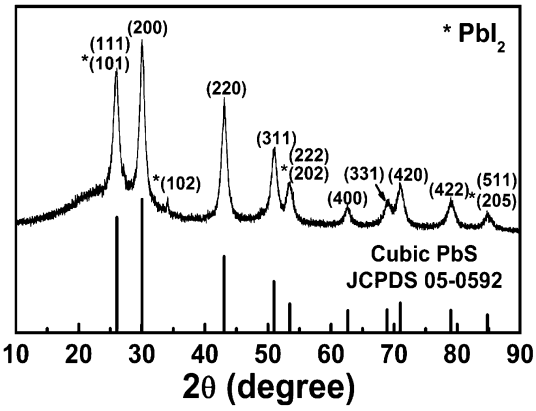

Figure 1. XRD pattern of the sample prepared by the reaction of $K[PbI_3]$ with TAA under typical synthesis conditions. The diffraction peaks marked with asterisks are attributed to PbI_2.

The morphology and microstructure of the PbS/PbI_2 nanocomposites were characterized by TEM and HRTEM. The TEM images of PbS/PbI_2 are shown in Figure 2A,B (Figure S1 in the SI shows a magnified version of Figure 2A,B). Figure 2A shows that the prepared particles have an irregular chainlike shape with diameters that range primarily from 25 to 40 nm. The higher-magnification TEM image (Figure 2B) shows numerous smaller dark particles of approximately 4−8 nm in size dispersed in the larger particles. HRTEM analysis (Figure 2C) clearly shows the lattice fringes of the nanocomposites. The fringe spacings are approximately 0.34, 0.30, and 0.26 nm, which match the interplanar spacings of PbI_2 (101), PbS (200), and PbI_2 (102), respectively. In addition, the elemental mapping (Figure 3) indicates that PbS and PbI_2 are distributed throughout the entire nanostructures, in agreement with the TEM and HRTEM observations.

The amount of PbI_2 in the nanocomposites was determined by EDS spectrum (Figure 4). The resultant Pb:S:I atomic ratio was approximately 33:31:2, which corresponds to 6 wt % PbI_2.

Compositional information was also obtained via XPS analysis. Figure 5A shows the XPS spectrum of the PbS/PbI_2 nanocomposites. The peaks located at 20.3, 137.11, 141.97, 413, 435.8, and 644.8 eV correspond to Pb $5d_{5/2}$, Pb $4f_{7/2}$, Pb $4f_{5/2}$, Pb $4d_{5/2}$, Pb $4d_{3/2}$, and Pb $4p_{3/2}$, respectively. The peaks at 161.2 and 225.5 eV correspond to S 2p and S 2s, respectively, and the peaks at 618.5 and 630 eV correspond to I $3d_{5/2}$ and $3d_{3/2}$, respectively. The XPS spectra and corresponding peak deconvolutions of the Pb 4f region and both the S 2p and I 3d core-level regions are shown in parts B−D of Figure 5, respectively. The Pb $4f_{7/2}$ BEs at 137.6 and 142.5 eV in Figure 5B are assigned to Pb−S bonds, whereas those at 137.8 and 142.8 eV are assigned to Pb−I bonds. All of the BEs observed for Pb, S, and I agree well with the literature values for PbS and PbI_2.[28−30] According to the Pb 4f, S 2p, and I 3d peak intensities, the Pb:S:I atomic ratio is approximately 13:12:1,

dx.doi.org/10.1021/ic501128n | Inorg. Chem. 2014, 53, 8548−8554

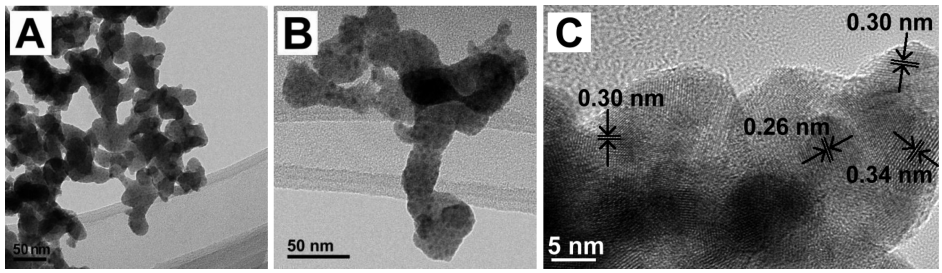

Figure 2. Lower (A) and higher (B) magnification TEM and HRTEM (C) images of the PbS/PbI_2 nanocomposites.

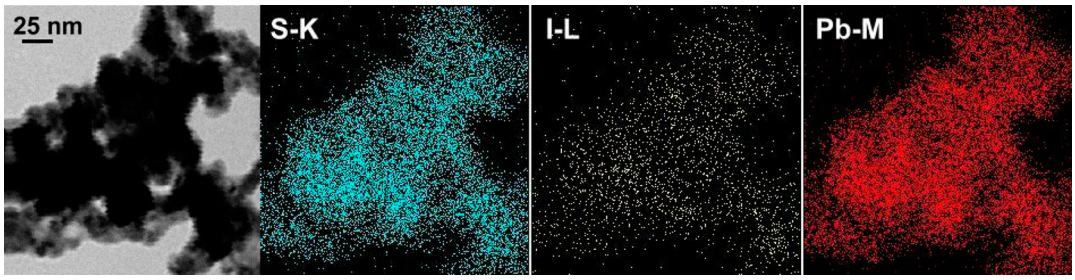

Figure 3. S, I, and Pb elemental mapping images of the PbS/PbI_2 nanocomposites.

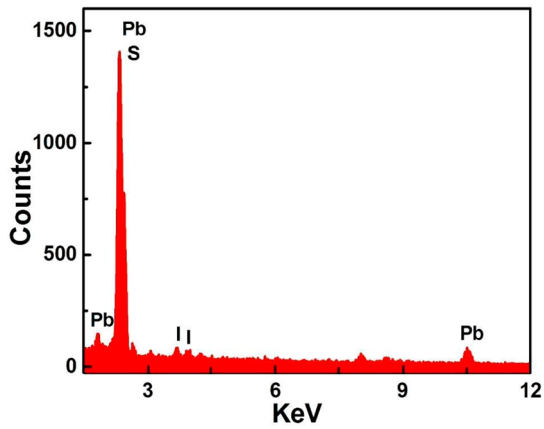

Figure 4. EDS spectrum of the PbS/PbI_2 nanocomposites prepared under the typical synthesis conditions.

which corresponds to 7.4 wt % PbI_2 and is consistent with the EDS results.

Water-soluble $Pb(CH_3COO)_2$ and $Pb(NO_3)_2$ are typically used as lead sources for the fabrication of lead chalcogenide nanocrystals. Recently, lead chalcogenide single-source precursors have been used to synthesize the corresponding lead chalcogenides.[31,32] In the present case, $K[PbI_3]$ was used as a source of both lead and iodine; it is soluble in acetone but insoluble and decomposable in water. The direct precipitation of $[PbI_3]^-$ with S^{2-} ions cannot occur in acetone because TAA cannot release its S^{2-} ions into this solvent without water. When water is added to an acetone solution of $K[PbI_3]$, $K[PbI_3]$ decomposes easily to generate PbI_2. In other words, PbI_2 is formed at an earlier stage of the PbS/PbI_2 composite material during growth in solution, which can be confirmed by the following experiment. When water is added to a $K[PbI_3]$/tartaric acid/acetone solution at 45 °C, chainlike aggregates composed of PbI_2 particles approximately 3−5 nm in size are formed (Figure S2 in the SI). A series of acetone/water volume-ratio-based control experiments were performed and revealed that PbS/PbI_2 nanocomposites with differing component ratios can be prepared by adjusting the amount of water added. As previously mentioned, nanocomposites with 6 wt % PbI_2 were obtained under the typical synthesis conditions (i.e., an acetone/water volume ratio of 2:1). When all other conditions were held constant and the acetone/water volume ratio was changed to 5:1 or 1:1, the PbI_2 weight percent was approximately 13% or 2%, respectively (Figure S3 in the SI). Furthermore, adjustment of the acetone/water volume ratio to 1:2 resulted in the formation of spherical PbS particles with size of approximately 20 nm. The causes of these differences may be as follows. The solubility product constant of PbS is much smaller than that of PbI_2 (PbS, 3.1×10^{-28}; PbI_2, 9.8×10^{-9}). Thus, it is key to controlling the S^{2-} ion concentration; otherwise, PbI_2 would easily convert to PbS through anion exchange. The PbI_2 weight percent varies with the acetone/water volume ratio because the use of additional water (i.e., large water/acetone volume ratios) leads to the increased dissolution of PbI_2 and the formation of more S^{2-} ions. Also, upon an increase in the content of water in the mixed solvent, the polarity of the solution increases[33] and the solubility of PbI_2 increases, leading to the PbI_2 amount decreasing in the final products. These combined effects result in relatively little PbI_2 and more PbS in the nanocomposites. So, the water/acetone ratio determines the contents of PbI_2 in the final products.

In addition, Gadakh and Bhosale reported that tartaric acid acted as a structure-directing agent and induced Sb_2S_3 nanorod formation.[34] In the present strategy, PbS/PbI_2 nanocomposites were obtained using a combination of tartaric acid and NaOH to adjust the solution acidity and control the hydrolyses of TAA to S^{2-} ions. The use of tartaric acid yields PbI_2 in the final product. If tartaric acid is not used and other conditions are held constant, only cubic PbS particles with about 18 nm size form (Figure 6). The use of twice the typical tartaric acid yields nanocomposites containing approximately 9 wt % PbI_2. Also, the shapes of the two products shown in Figure 2A and Figure 6 are markedly different, which may result from the complex action of tartaric acid on the lead(II) species to direct the formation of irregular chainlike particles. Thus, tartaric acid

dx.doi.org/10.1021/ic501128n | Inorg. Chem. 2014, 53, 8548−8554

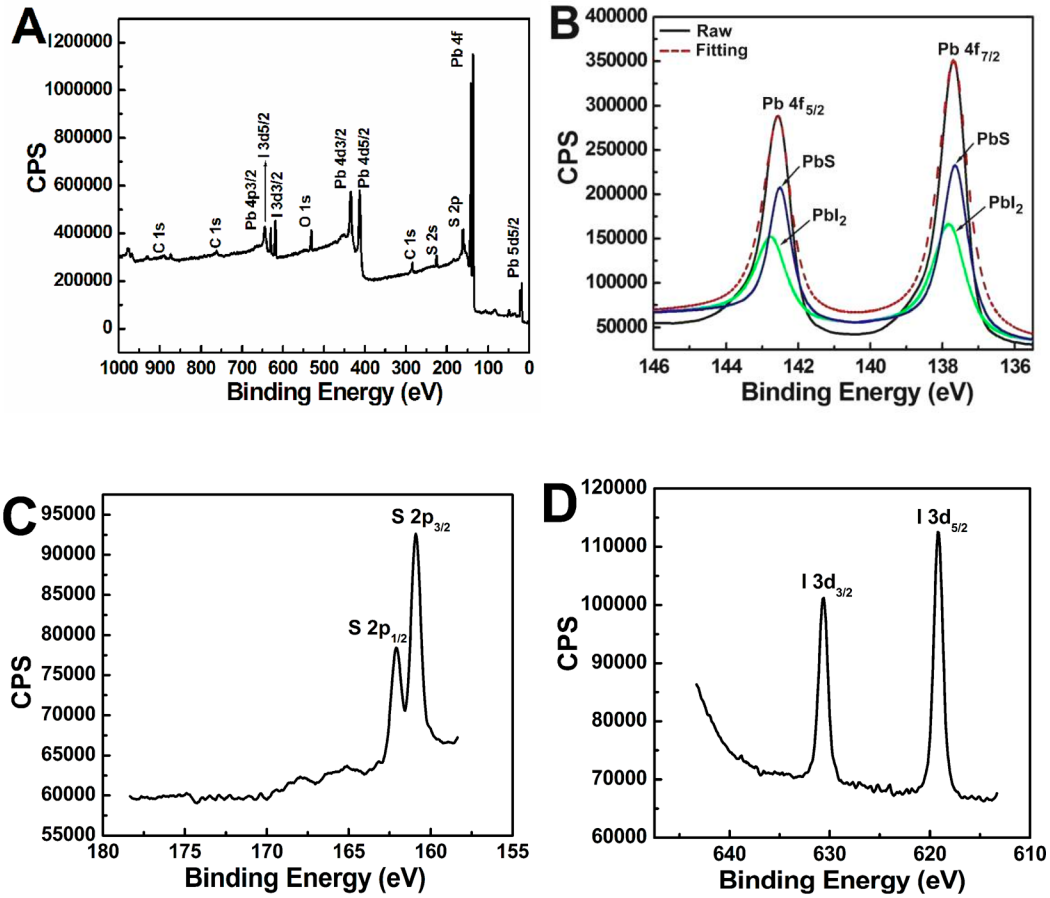

Figure 5. XPS spectra for the PbS/PbI_2 nanocomposites: (A) typical XPS spectrum of the nanocomposites and high-resolution XPS scans for Pb 4f (B), S 2p (C), and I 3d (D) cores, respectively.

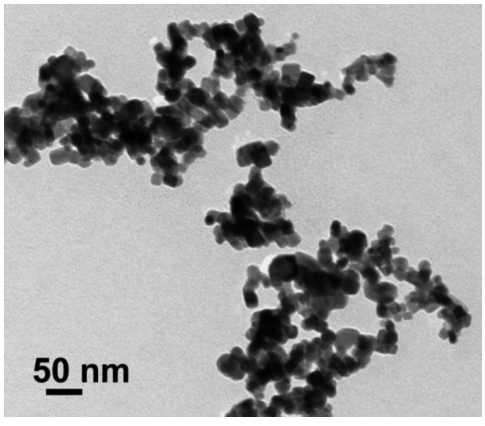

Figure 6. TEM image of PbS particles obtained in the absence of tartaric acid and keeping other typical conditions constant.

plays a dual role in the present strategy during formation of the PbS/PbI_2 nanocomposites.

It is worth pointing out that this simple bicomponent precursor-based reaction route can be extended to prepare other lead-containing nanocomposites. For example, when using ammonia or selenourea instead of TAA and keeping other reaction conditions constant as in the case for PbS/PbI_2, the Pb_3O_4/PbI_2 or PbSe/PbI_2 nanocomposites can be obtained. The corresponding TEM images and EDS spectra of these two nanocomposites are shown in Figure 7.

The reduced or oxidized semiconductor nanocrystals generated under a certain electrode potential can react with redox-active coreactants to yield the excited state and produce ECL.[35] In our previous work, we reported that PbSe nanostructures exhibited good ECL properties.[36,37] To date, PbS-based ECL has rarely been studied.[38] In the present work, the ECL performances of both PbS and PbS/PbI_2 are tested in CH_2Cl_2 containing 0.1 M tetra-*n*-butylammonium perchlorate (TBAP). We fabricate the working electrodes by depositing the samples onto a pretreated GCE. Light emission is observed when the electrode potential is cycled between −1.5 and +1.5 V at a scan rate of 100 mV s^{-1}. The emissions of a bare GCE and a PbI_2-modified electrode are also evaluated for comparison. No ECL emissions are observed for the bare GCE (figure not shown), and the PbI_2-modified electrode exhibits a couple of low-intensity reduction and oxidation peaks at approximately −1.0 and +1.4 V (vs Ag/AgCl; plot a in Figure 8). This result is likely due to the large band gap of PbI_2 (E_g > 2 eV), which is disadvantageous to electronic transitions. PbS exhibits reduction and oxidation peaks at approximately −1.15 and +1.5 V (vs Ag/AgCl; plot b in Figure 8), which correlates to lowest unoccupied molecular orbital and highest occupied molecular orbital electron transfer, respectively.[37] PbS can form a reduced ($PbS^{\bullet-}$) and an oxidized ($PbS^{\bullet+}$) species during the potential cycling. Two oppositely charged PbS species can collide to produce an excited state (PbS*), which generates luminescence. Two emission peaks near −1.0 and +1.35 V (vs Ag/AgCl) were observed for PbS/PbI_2 (plot c in Figure 8), and their intensities were approximately 2-fold higher than those of

dx.doi.org/10.1021/ic501128n | *Inorg. Chem.* 2014, 53, 8548−8554

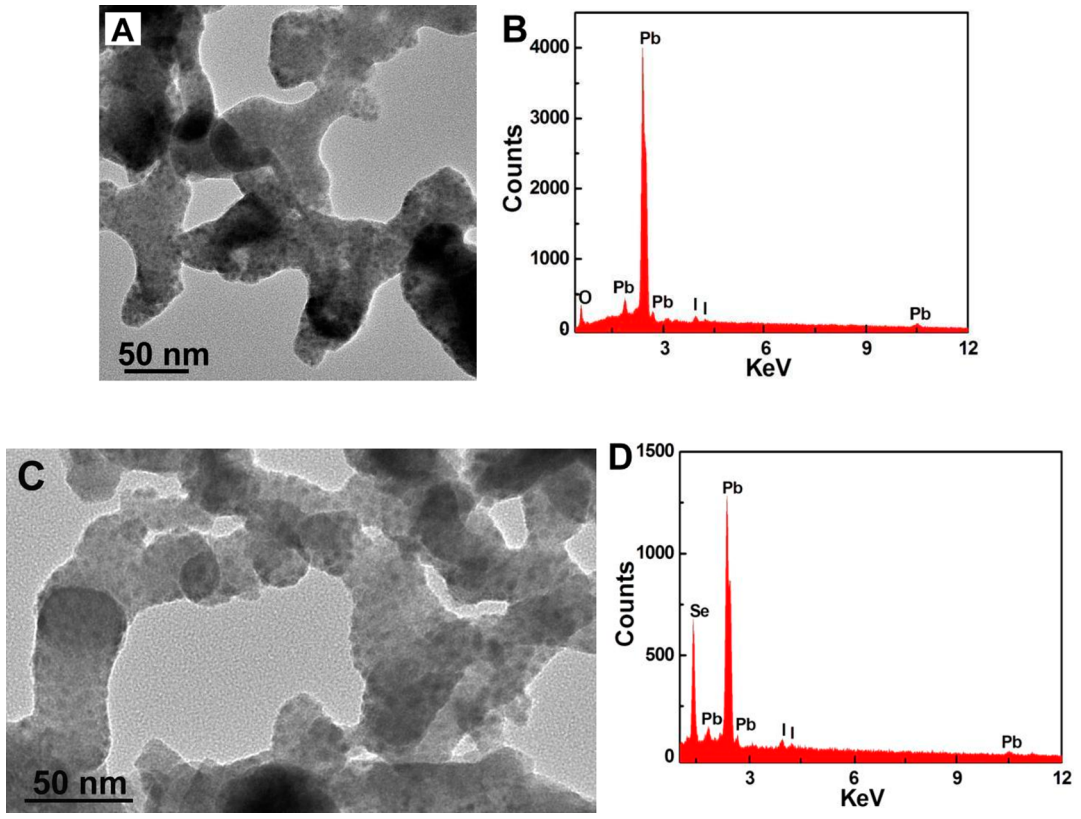

Figure 7. TEM images (A and C) and EDS spectra (B and D) of the Pb_3O_4/PbI_2 (A and B) and $PbSe/PbI_2$ (C and D) nanocomposites.

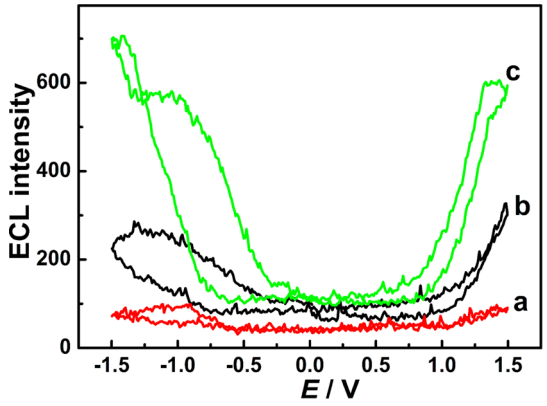

Figure 8. ECL intensities for PbI_2 (a), PbS (b), and PbS/PbI_2 (6 wt % PbI_2) (c) in CH_2Cl_2 containing 0.1 M TBAP. Scan rate: 0.1 V s^{-1}.

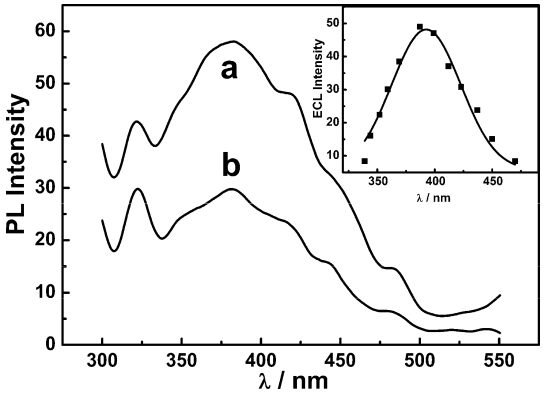

Figure 9. PL spectra of PbS/PbI_2 (6 wt % PbI_2) (a) and PbS (b), respectively. Excitation was at λ_{ex} = 290 nm. Inset: ECL spectrum of PbS/PbI_2 (6 wt % PbI_2).

PbS. To determine why the ECL properties of PbS/PbI_2 are better than those of PbS, photoluminescence (PL; Figure 9) of these two products has been done. PbS exhibited a maximum absorption at 382 nm. After PbS was doped with PbI_2, this peak did not shift, which indicated that fluorescence did not result from Förster resonance energy transfer. In addition, the PL intensity for PbS/PbI_2 was greater than that for PbS, similar to the case of ECL. The ECL spectra of PbS/PbI_2 showed emission peak positions at 391 nm (inset in Figure 9), which indicated that the surface of PbS/PbI_2 was efficiently passivated.[39] The PL decay curves for PbS/PbI_2 and PbS in $CHCl_3$ are shown in Figure 10. PbS/PbI_2 exhibits an excitation lifetime of 0.037 ns, whereas PbS has an excitation lifetime of 0.102 ns. The shorter PbS/PbI_2 lifetime relative to that of PbS indicates that the PbS/PbI_2 energy decay is lower and that the PL efficiency is greater, which results in greater PL intensity. This result may be induced by the heavy-atom effect of iodine.[40]

Interestingly, the ECL properties of the PbS/PbI_2 nanocomposites are related to the amount of the PbI_2 component. The effect of differing PbI_2 weight percents on the ECL of PbS is preliminarily investigated (Figure 11). The emission peak locations of these three samples are approximately identical, whereas their ECL intensities differ substantially. The ECL intensity of the composite is greatest when the amount of PbI_2 in the composite is moderate (6 wt % PbI_2). The reason for this behavior might be the differences in the quantum efficiencies: PbS/PbI_2 (6 wt % PbI_2) exhibits an excitation lifetime of 0.037 ns, whereas PbS/PbI_2 (2 wt % PbI_2) has an excitation lifetime of 0.149 ns.

dx.doi.org/10.1021/ic501128n | Inorg. Chem. 2014, 53, 8548−8554

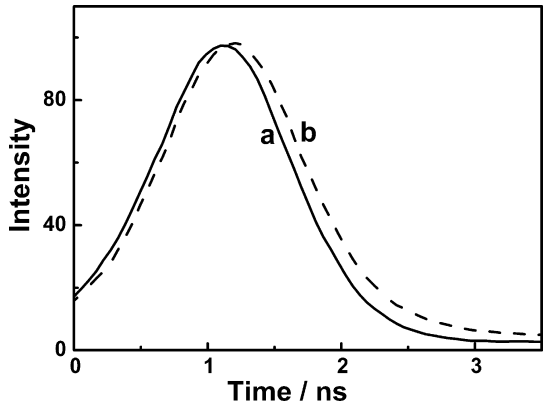

Figure 10. PL decay curves of PbS/PbI_2 (6 wt % PbI_2) (a) and PbS (b) in a $CHCl_3$ solution. Excitation was at λ_{ex} = 290 nm.

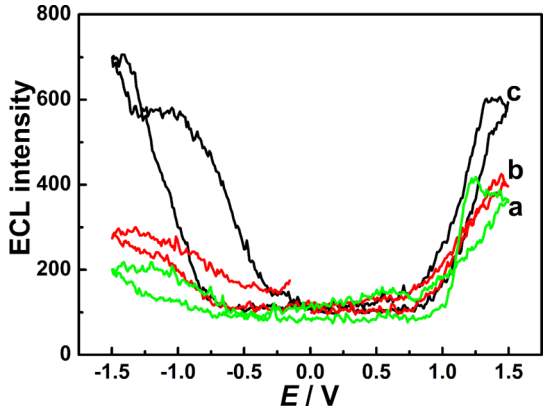

Figure 11. ECL intensities for PbS/PbI_2 (2 wt % PbI_2) (a), PbS/PbI_2 (13 wt % PbI_2) (b), and PbS/PbI_2 (6 wt % PbI_2) (c) in CH_2Cl_2 containing 0.1 M TBAP. Scan rate: 0.1 V s^{-1}.

The effect of the amount of materials on the electrode on the ECL intensity of the PbS/PbI_2 nanocomposites was evaluated. With an increase in the PbS/PbI_2 nanocomposite colloid solution volume, the peak current increased. When 2 μL of the PbS/PbI_2 nanocomposite colloid solution was dropped onto the pretreated GCE surface, the maximum ECL intensity was obtained. Upon a further increase in the colloid solution volume, the ECL intensity decreased. Thus, the optimal volume of the PbS/PbI_2 nanocomposite colloid solution was 2 μL.

Figure 12 shows the ECL emission from the PbS/PbI_2 (6 wt % PbI_2) modified electrode under continuous potential scanning for six cycles. No obvious changes are observed, which indicates that the ECL of PbS/PbI_2 is stable. This stable and sensitive ECL response is attractive for ECL sensing applications. The reproducibility was confirmed in five measurements with a relative standard deviation (RSD) of 7.6%. The fabrication reproducibility of five electrodes, made independently, showed an acceptable reproducibility with RSD of 5.3%. Further work on the design of novel biosensors based on the ECL emission of PbS/PbI_2 is ongoing in our laboratory.

4. CONCLUSIONS

In summary, a simple bicomponent precursor-based approach to the synthesis of PbS/PbI_2 nanocomposites was developed. $K[PbI_3]$ was chosen as the source of both lead and iodine for these nanocomposites. The PbI_2 content in these composites could be varied to some extent by changing the water/acetone

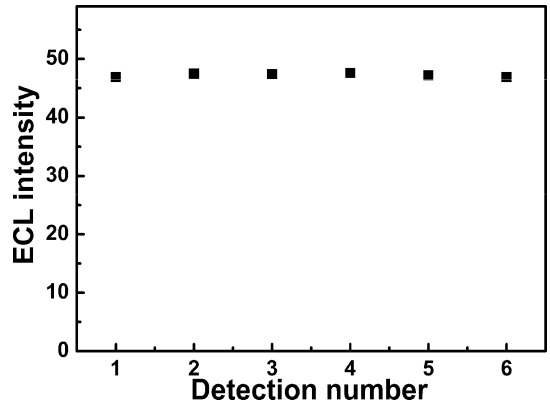

Figure 12. ECL emissions from PbS/PbI_2 in CH_2Cl_2 containing 0.1 M TBAP at a potential of 1.35 V over six cycles. Scan rate: 0.1 V s^{-1}. Scan range: −1.5 to +1.5 V.

ratio. The PbS/PbI_2 nanocomposite-modified electrodes exhibited interesting ECL performance, with ECL intensities that varied with the amount of PbI_2. This behavior may be attributable to the heavy-atom effect of iodine. This facile synthetic method can be extended to prepare other lead-containing nanocomposites and is of great potential toward the design and synthesis of advanced nanomaterials with specific properties for functional applications.

■ ASSOCIATED CONTENT

Ⓢ Supporting Information

Table of different volume ratios of acetone to water used to synthesize samples and TEM images and EDS spectra of PbS/PbI_2 nanocomposites. This material is available free of charge via the Internet at http://pubs.acs.org.

■ AUTHOR INFORMATION

Corresponding Authors

*E-mail: daizhihuii@njnu.edu.cn.

*E-mail: baojianchun@njnu.edu.cn.

Notes

The authors declare no competing financial interest.

■ ACKNOWLEDGMENTS

This work was supported by the National Natural Science Foundation of China for the project (Grants 21175069 and 21171096) and a Research Fund for the Doctoral Program of Higher Education of China (Grant 20113207110005). The authors greatly appreciate financial support from the Priority Academic Program Development of Jiangsu Higher Education Institutions and the Jiangsu Collaborative Innovation Center of Biomedical Functional Materials.

■ REFERENCES

(1) Kershaw, S. V.; Susha, A. S.; Rogach, A. L. *Chem. Soc. Rev.* **2013**, *42*, 3033−3087.

(2) Kim, S.; Fisher, B. R.; Eisler, H. J.; Bawendi, M. G. *J. Am. Chem. Soc.* **2003**, *125*, 11466−11467.

(3) Jian, P. K.; Huang, X. H.; El-Sayed, M. A. *Acc. Chem. Res.* **2008**, *41*, 1578−1586.

(4) Burda, C.; Chen, X.; Narayanan, R.; El-Sayed, M. A. *Chem. Rev.* **2005**, *105*, 1025−1102.

(5) Maturova, K.; Nanayakkara, S. U.; Luther, J. M.; Lagemaat, J. V. D. *Nano Lett.* **2013**, *13*, 2338−2345.

(6) Mokari, T.; Habas, S. E.; Zhang, M. J.; Yang, P. D. *Angew. Chem., Int. Ed.* **2008**, *47*, 5605−5608.
(7) Shevchenko, E. V.; Talapin, D. V.; Kotov, N. A.; O'Brien, S.; Murray, C. B. *Nature* **2006**, *439*, 55−59.
(8) Regulacio, M. D.; Han, M. Y. *Acc. Chem. Res.* **2010**, *43*, 621−630.
(9) Shi, J.; Gider, S.; Babcock, K.; Awschalom, D. D. *Science* **1996**, *271*, 937−941.
(10) Sun, L.; Koh, Z. Y.; Wang, Q. *Adv. Mater.* **2013**, *25*, 4598−4604.
(11) Winiarz, J. G.; Zhang, L.; Park, J.; Prasad, P. N. *J. Phys. Chem. B* **2002**, *106*, 967−970.
(12) Shi, Y.; Li, H.; Wang, L.; Shen, W.; Chen, H. *ACS Appl. Mater. Interfaces* **2012**, *4*, 4800−4806.
(13) Wang, H. B.; Kubo, T.; Nakazaki, J.; Kinoshita, T.; Segawa, H. *J. Phys. Chem. Lett.* **2013**, *4*, 2455−2460.
(14) Bubenhofer, S. B.; Schumacher, C. M.; Koehler, F. M.; Luechinger, N. A.; Grass, R. N.; Stark, W. J. *J. Phys. Chem. C* **2012**, *116*, 16264−16270.
(15) Fang, F.; Zhao, D. X.; Li, H. B.; Zhang, Z. Z.; Zhang, J. Y.; Shen, D. Z. *Appl. Phys. Lett.* **2008**, *93*, 233115.
(16) Wang, X.; Liu, G.; Lu, G. Q.; Cheng, H. M. *Int. J. Hydrogen Energy* **2010**, *35*, 8199−8205.
(17) Ma, W.; Luther, J. M.; Zheng, H.; Wu, Y.; Alivisatos, A. P. *Nano Lett.* **2009**, *9*, 1699−1703.
(18) Acharya, K. P.; Khon, E.; O'Conner, T.; Nemitz, I.; Klinkova, A.; Khnayzer, R. S.; Anzenbacher, P.; Zamkov, M. *ACS Nano* **2011**, *5*, 4953−4964.
(19) Luther, J. M.; Zheng, H.; Sadtler, B.; Alivisatos, A. P. *J. Am. Chem. Soc.* **2009**, *131*, 16851−16857.
(20) Mukherjee, B.; Peterson, A.; Subramanian, V. *Chem. Commun.* **2012**, *48*, 2415−2417.
(21) Lee, J. S.; Shevchenko, E. V.; Talapin, D. V. *J. Am. Chem. Soc.* **2008**, *130*, 9673−9675.
(22) Zhuang, T. T.; Fan, F. J.; Gong, M.; Yu, S. H. *Chem. Commun.* **2012**, *48*, 9762−9764.
(23) Chang, Y. C.; James, R. B. *Phys. Rev. B* **1997**, *55*, 8219−8225.
(24) Nair, G.; Chang, L. Y.; Geyer, S. M.; Bawendi, M. G. *Nano Lett.* **2011**, *11*, 2145−2151.
(25) Sandroff, C. J.; Kelty, S. P.; Hwang, D. M. *J. Chem. Phys.* **1986**, *85*, 5337.
(26) Dag, I.; Lifshitz, E. *J. Phys. Chem.* **1996**, *100*, 8962−8972.
(27) Kasi, G. K.; Dollahon, N. R.; Ahmadi, T. S. *J. Phys. D: Appl. Phys.* **2007**, *40*, 1778.
(28) Pawar, S. B.; Shaikh, J. S.; Devan, R. S.; Ma, Y. R.; Haranath, D.; Bhosale, P. N.; Patil, P. S. *Appl. Surf. Sci.* **2011**, *258*, 1869−1875.
(29) Wang, Z.; Pan, L.; Hu, H.; Zhao, S. *CrystEngComm* **2010**, *12*, 1899−1904.
(30) Zheng, Z.; Liu, A. R.; Wang, S. M.; Wang, Y.; Li, Z. S.; Lau, W. M.; Zhang, L. Z. *J. Mater. Chem.* **2005**, *15*, 4555−4559.
(31) Boadi, N. O.; Malik, M. A.; O'Brien, P.; Awudza, J. A. M. *Dalton Trans.* **2012**, *41*, 10497−10506.
(32) Planet, I. J. L.; Zeid, T. W.; Yang, P. D.; Mokari, T. *J. Mater. Chem.* **2010**, *20*, 6612−6617.
(33) Han, Y. C.; Liu, S. H.; Han, M.; Bao, J. C.; Dai, Z. H. *Cryst. Growth Des.* **2009**, *9*, 3941−3947.
(34) Gadakh, S. R.; Bhosale, C. H. *Mater. Chem. Phys.* **2003**, *78*, 367−371.
(35) Bard, A. J.; Faulkner, L. R. *Electrochemical Methods*, 2nd ed.; Wiley: New York, 2001.
(36) Han, M.; Li, Y. R.; Niu, H. Y.; Liu, L. L.; Chen, K. J.; Bao, J. C.; Dai, Z. H.; Zhu, J. M. *Chem.—Eur. J.* **2011**, *17*, 3739−3745.
(37) Sun, L.; Bao, L.; Hyun, B. R.; Bartnik, A. C.; Zhong, Y. W.; Reed, J. C.; Pang, D. W.; Abruña, H. D.; Malliaras, G. G.; Wise, F. W. *Nano Lett.* **2009**, *9*, 789−793.
(38) Haram, S. K.; Quinn, B. M.; Bard, A. J. *J. Am. Chem. Soc.* **2001**, *123*, 8860−8861.
(39) Myung, N.; Bae, Y.; Bard, A. J. *Nano Lett.* **2003**, *3*, 1053−1055.
(40) Cowan, D. O.; Drisko, R. L. E. *J. Am. Chem. Soc.* **1970**, *92*, 6281−6285.